

Coupled electron-phonon transport and heat transfer pathways in graphene nanostructures



Liang Chen ^{a,*}, Zhequan Yan ^b, Satish Kumar ^b

^a School of Energy and Power Engineering, Xi'an Jiaotong University, Xi'an, Shaanxi 710049, China

^b G. W. Woodruff School of Mechanical Engineering, Georgia Institute of Technology, Atlanta, GA 30332, United States

ARTICLE INFO

Article history:

Received 17 May 2017

Received in revised form

8 July 2017

Accepted 25 July 2017

Available online 3 August 2017

ABSTRACT

A hybrid Boltzmann transport equation model coupled with a two-temperature model is developed to simulate the heat dissipation in single layer graphene (SLG) suspended or supported on SiO₂ and with/without Cu contacts. This hybrid model includes the phonon transport in SLG, electron-phonon interaction (EPI) in SLG, and phonon/electron transmission at the interface between SLG and its surroundings. The EPI strength between electrons and various phonon modes is obtained at different temperatures using first-principle calculations. Simulations are performed for SLG with different graphene lengths, contact configurations and heating powers. For the SLG suspended on SiO₂, adding Cu contact at ends can remarkably improve the heat dissipation and lower the maximum temperature in SLG, especially at small lengths of SLG. The SLG/Cu interface can still be the major heat dissipation pathway when its contact area is similar with that of SLG/SiO₂ interface, which can be attributed to the higher thermal conductivity of Cu. For the SLG fully supported on SiO₂, adding Cu contact can effectively lower the temperature in SLG of small length, but the dominating heat dissipation pathway will be shifted from SLG/Cu interface to SLG/SiO₂ interface as the SLG length increases.

© 2017 Elsevier Ltd. All rights reserved.

1. Introduction

Due to the exceptional properties such as high electron mobility, high thermal conductivity and high Young's modulus, graphene has been widely investigated for many applications. The intrinsic thermal conductivity of graphene has been reported as high as 2000–5300 W/mK at room temperature by many experimental [1–3] and numerical studies [4–7]. In electronic devices for high-field applications, the use of graphene can significantly increase the current carrying capacity. But the current-induced breakdown of device is still thermally activated, and the effective heat dissipation in graphene is critical for the thermal management [8–10]. The dominant heat carriers in graphene are phonons, and their interaction with electrons plays an important role in the heat dissipation in graphene based devices.

The heat transfer from graphene nanostructure to its surrounding may have unique characteristics which should be taken into account in the models employed for the thermal transport study. Firstly, due to the 2D structure of graphene, the phonon

transport exhibits strong mode dependent behavior which is due to the large difference in the mean free path (MFP) of the acoustic and optical phonons. In the pristine single layer graphene (SLG), the out-of-plane acoustic (ZA) modes have MFP in micrometers [5,11], the longitudinal and transverse acoustic modes have relatively smaller MFP, but the optical modes have one to two orders of magnitude smaller MFP than the acoustic modes [12,13]. A model that accounts for the contributions of different modes is needed for the investigation of thermal transport in graphene. Secondly, the thermal transport in graphene devices involves different carriers such as electrons and phonons, and the energy exchange between them can have significant impact on the heat transfer [9]. Graphene makes contact with complex surroundings including dielectrics and metals in its electronic devices. Because of the different heat carriers involved and different interface properties with different contacts, exploration of the interfacial thermal transport mechanism gets complicated. Phonons are the major heat carriers at the graphene and dielectric substrate interface [14], while both phonons and electrons as well as their interactions are important at the graphene and metal-electrode interface [15–18]. Because of the long phonon MFP but small size of graphene considered, the boundary scattering can suppress the thermal conductivity even at

* Corresponding author.

E-mail address: liangchen@mail.xjtu.edu.cn (L. Chen).

room temperature [19,20]. The size effects and boundary scattering should be carefully considered for graphene with different phonon modes of various MFPs [21].

Raman technique [1,22] is widely used for the characterization of structural, electrical, thermal and optical properties of graphene, such as the measurement of number of graphene layers [23], the stacking order of multilayer graphene (MLG) [24,25], the crystallographic orientation of graphene [26], the thermal conductivity [1,22], the effect of strain [27], and doping on properties [28]. During Raman measurements, the energy is transferred to electrons via inelastic scattering of photons at femtosecond time scale. The following energy relaxation involves electron-electron collisions at femtoseconds scale and electron-phonon scattering at picoseconds scale [29,30]. The heat absorbed by electrons is transferred to phonons via electron-phonon interactions (EPI), followed by the phonon-dominated thermal transport in graphene and heat dissipation to its surroundings such as substrate and metal contacts. A detailed study of the energy exchange between electrons and phonons can benefit the interpretation of the related experimental measurements.

Understanding of the heat dissipation in graphene and from graphene to its surroundings (e.g., metal and SiO₂) is critical for the efficient thermal management of graphene nano-electronics and the interpretation of experimental measurements such as by using Raman technique. In the previous studies, various models based on Boltzmann transport equation (BTE) have been developed to study the thermal transport in SLG and MLG. The studies [5,11,31] include both the normal and Umklapp scattering process in the BTE model which demonstrated that the ZA modes could dominate the thermal transport in suspended SLG. The dominant contribution from ZA modes can be attributed to the large density of flexural phonons associated with the quadratic ZA branch dispersion, and the restricted phase space for the ZA phonon scattering. The breaking of the reflection symmetry of the two-dimensional graphene can significantly suppress the ZA contribution [5]. However, several studies indicate the contribution from longitudinal acoustic (LA) and transverse acoustic (TA) could dominate the thermal conductivity of SLG. According to recent BTE [5,11,31] simulations, the significant reduction of thermal conductivity of supported SLG or MLG can be explained by the suppression of acoustic modes due to the SLG-substrate interaction or the interlayer interaction.

Although there are many BTE studies on the thermal transport of graphene, only few study has focused on the thermal transport in the graphene nanostructures considering the effects of all contacts in its electronic devices [5,11,32]. The computational cost to solve the BTE model depends on the methodology to describe phonon scattering and the system dimension. For SLG and MLG, simulations based on the detailed BTE models can be performed in a computational domain up to a size of micrometers to millimeters. However, simplifications and assumptions have to be made in order to solve the thermal transport problem in a configuration including contacts. Hybrid BTE models which combine BTE with Fourier conduction equation have been used in the previous studies on nano-electronic devices such as GaN transistors [33,34]. In the hybrid BTE, the thermal transport by the optical band or away from the ballistic transport region is usually described by the Fourier conduction equation which can help to significantly reduce the computational cost and allow the simulation at device scale. For graphene based nano-scale devices, the hybrid BTE model should appropriately consider the phonon transport in graphene, EPI in graphene, and phonon/electron transmission at the interface between graphene and its surroundings.

In this study, a computational model based on the Boltzmann transport equations is developed to study the coupled electron-phonon transport in SLG supported on SiO₂ substrate and with

metal contacts at ends. The heat dissipation through SLG/substrate and SLG/metal interfaces are quantified, and their dependence on SLG length and heating power is demonstrated. SLG/metal interface is found to be an important heat dissipation pathway at small SLG length due to the strong non-equilibrium between electrons and phonons. The findings of this study provide insights into the electron-phonon coupled transport mechanism and helps to understand the heat transfer pathways in graphene-based nano-electronics.

2. Methodology

In order to take into account the multiphysics characteristics of the energy transport in graphene, a computational model is developed using a diffusive equation for electrons and non-gray Boltzmann transport equations for phonons. The two-temperature model (TTM) proposed by Anisimov et al. [35] is employed to describe the electron-phonon coupled transport in metal. The TTM consists of diffusion and source terms, and the electron-phonon coupling factor is used in the source term to represent the rate of the energy exchange between electrons and lattice [36]. The calculation of the electron-phonon coupling factor will be discussed in the following section. The non-gray BTE model used for the phonon transport in SLG considers all phonon modes, but usually employs the single-mode relaxation time (SMRT) approximation [37,38]. Moreover, the BTE-SMRT approach can include the mode dependencies of both the phonon transport and EPI. The model requires several important parameters including mode-dependent phonon lifetime, EPI parameter, electron transmission, and phonon transmission. This section will briefly introduce the hybrid model as well as the methodology to determine these parameters. A complete description of the model parameters

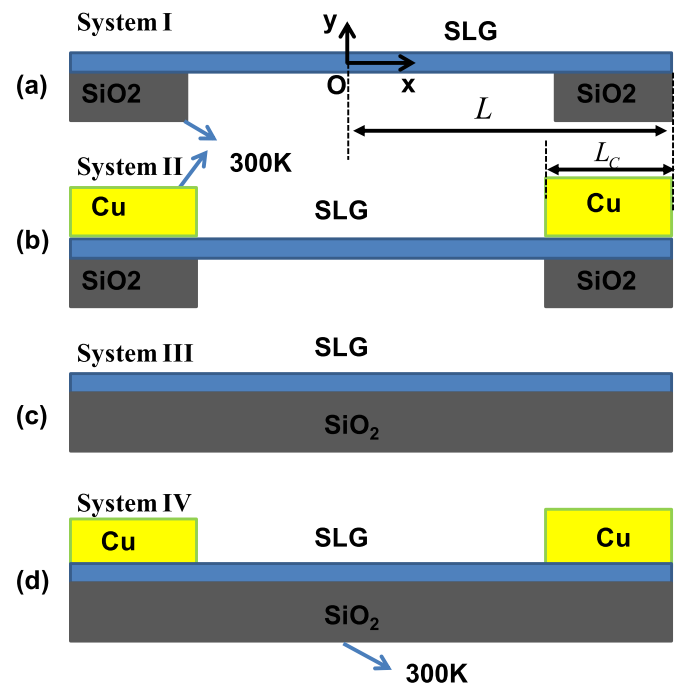


Fig. 1. Schematic of the different configurations considered for the simulations (a) System I: SLG suspended on SiO₂; (b) System II: SLG suspended on SiO₂ with Cu contacts; (c) System III: SLG supported on SiO₂ substrate; (d) System IV: SLG supported on SiO₂ substrate with Cu contacts. L denotes the half length of SLG which varies from 24.5 nm–490 nm in current work. L_c denotes the contact length (9.8 nm) with Cu in (b) and (d), and SiO₂ in (a) and (b). (A colour version of this figure can be viewed online.)

and implementation can be found in the supplementary document.

Fig. 1 shows the different configurations considered in the present work for thermal transport study: System I consists of SLG suspended on SiO₂, System II consists of SLG suspended on SiO₂ with Cu contacts, System III consists of SLG supported on SiO₂ substrate, and System IV consists of SLG supported on SiO₂ substrate with Cu contacts. The heat source is applied in SLG in the center of the device. Considering the symmetry of the structures, only right half of the device is simulated for all cases, as shown in Fig. 1 (a).

In Fig. 1 (a), (b) and (d), the contact length between SLG and Cu or SiO₂ is set at 9.8 nm. The length of the simulated structures (half of the device length as shown in Fig. 1) varies from 24.5 nm to 490 nm. The heat absorbed by electrons in SLG is assumed to follow Gaussian distribution in x direction, e.g., $P(x) = I/(\sqrt{2\pi}\sigma) \cdot e^{-x^2/\sigma^2}$. In electronic devices, the hot spots have sizes ranging from several nanometers to few microns depending on the channel length and strength of electric field [39,40]. For the short channel devices, decreasing dimensions lead to nanometer-scale hot spots [39,40]. In this study, the domain size is from 24.5 nm to 490 nm, and a heating region width (σ) of 4.9 nm (10% of largest size considered) is used in the simulations. A width of 424.35 nm is used to calculate the power density. The intensity I from 2×10^{-5} W to 10^{-4} W is selected so that the lattice temperature in the simulations falls in the range of interests (<600 K) for the study of hot spots in nano-electronics [41]. The corresponding power density ranges from 9.6×10^8 W/m² \sim 4.8×10^{10} W/m² which is 1–2 orders of magnitude higher than the average value ($\sim 1.4 \times 10^8$ W/m²) over the entire device [42].

2.1. Hybrid BTE model and electron-phonon interaction in graphene

In pristine graphene, the electron mean free path can be on order of micrometer [43,44]. However, previous studies [45,46] indicate that the electronic contribution to the thermal conductivity of graphene falls into the range of <1 W/mK to \sim 100 W/mK depending on the carrier density and temperature, which is certainly much lower than the phonon contribution. Therefore, the electron transport can be described by the diffusive equations, as shown in Eq. (1) [47].

$$\frac{\partial}{\partial x} \left(k_{el} \frac{\partial T_{el}}{\partial x} \right) - S + \sum_{q,v} E_{eph}(x, q, v) = 0 \quad (1)$$

where T_{el} , and k_{el} are the temperature, and effective thermal conductivity of electrons, respectively. The source term S includes the heat generation by Joule heating, and it also includes the interfacial energy exchange. The heat is then transferred to phonons via the electron-phonon energy exchange term, $E_{eph}(x, q)$, which is summed over all the phonon mode polarization v and wave vector q at a specific spatial cell x .

For solving the Boltzmann transport equation of phonons, various approximations for the phonon-phonon scattering term have been implemented with varying levels of accuracy. In the most complete form, this term should satisfy the conservation rules through the coupling of every phonon energy density to all the other phonons, and it has been implemented in several studies [5,20,48]. Application of such approach for simulating transport in a device structure can be computationally very expensive. The single mode relaxation time (SMRT) approximation uses the phonon relaxation time to represent the scattering of each phonon mode with all the others. Previous studies [5,48] show SMRT approach underestimates the thermal conductivity of pristine graphene, but still can capture the mode dependent phonon transport in a better

way than the gray and semi-gray BTE models. For graphene at high temperatures, the anharmonic scattering increases, and for graphene of nanometer size boundary scattering increases. The SMRT approach can provide a fairly good description in these conditions. In the present work, a hybrid multi-physics model involving graphene, substrate and metals, has been considered, so the implementation of the complete form of phonon BTE will be extremely time consuming. The SMRT approximation seems to be the best choice here considering the computational expense. For a phonon mode (q, v) , the BTE can be written as [38,49]:

$$\nabla \cdot (v_{ph} \hat{s} e_{ph}) - \frac{e_{ph}^{eq} - e_{ph}}{\tau_{ph}} - E_{eph} - S_{ph} = 0 \quad (2)$$

where e_{ph} , v_{ph} , and τ_{ph} are the energy density, group velocity, and lifetime of a phonon mode (q, v) , respectively. The interfacial heat flux by phonons is included in the source term S_{ph} . In order to reduce the computation cost, 14 bands are considered for each phonon polarization (discretization for q). In each phonon mode, the energy flux is determined by integrating over its wave vector band. Equations (3) and (4) show expression for non-equilibrium energy flux and equilibrium energy flux, respectively for a phonon mode with wave-vector q and polarization v . The subscripts, j, k , and l , are the indices for the band of wave-vector q , the azimuthal angle φ and the polarization v , respectively.

$$e_{j,k,l}'' = \frac{1}{(2\pi)^2} \int_{q_{j-1/2,k}}^{q_{j+1/2,k}} \int_{\varphi_{l-1/2}}^{\varphi_{l+1/2}} e_{ph}(q, v_k) q d\varphi dq \quad (3)$$

$$e_{j,k}''^{eq} = \frac{\delta\varphi}{2\pi} \frac{1}{(2\pi)^2} \int_{q_{j-1/2,k}}^{q_{j+1/2,k}} e_{ph}^{eq}(q, v_k) 2\pi q dq \quad (4)$$

The relaxation time of each phonon mode is determined using the spectral energy density method, and the details can be found in our previous work [50]. Owing to the long MFP of phonons in graphene, the size effects due to the boundary scattering should be appropriately addressed in the phonon transport model. We have considered the size effects by including the boundary scattering in the calculation of total scattering rate of different phonon modes using the Matthiessen's rule [21]. Moreover, as demonstrated in the previous works [11,51,52], the coupling between graphene and substrate has impact on the phonon lifetime as well as the thermal conductivity. For the calculation of the phonon lifetime of graphene supported on a substrate, we have included scattering due to the substrate, and then determined the total scattering rates of different phonon modes using the Matthiessen's rule. The details of the calculations of substrate scattering can be found in Ref. [11]. The phonon lifetime of different modes are compared between the free standing graphene and SiO₂ supported graphene. As shown in Fig. S1 in the supplementary material, the substrate scattering has significant effects on the low frequency acoustic phonons.

The energy exchange rate $E_{e-ph}(q, v)$ between electrons and phonons of (q, v) mode is determined using the coupling matrix $g_{mn}^v(\mathbf{k}, \mathbf{q})$, where m and n are the electronic band indices, v is the phonon polarization, and k and q are the wave vector for electron and phonon states, respectively [47,53,54].

$$E_{e-ph}(q, v) = \frac{8\pi}{\hbar} \sum_{m,n,\mathbf{k}} \hbar\omega_{\mathbf{q}v} |g_{mn}^v(\mathbf{k}, \mathbf{q})|^2 S(k, q) \delta(\varepsilon_{m\mathbf{k}+\mathbf{q}} - \varepsilon_{n\mathbf{k}} - \hbar\omega_{\mathbf{q}v}) \quad (5)$$

Here, the summation is over all electron bands mn and wave vectors k . $S(k, q)$ is the thermal factor that considers the equilibrium distribution of electrons and phonons.

$$S(k, q) = N_q f_k (1 - f_{k+q}) - (N_q + 1) f_{k+q} (1 - f_k) \quad (6)$$

where f_k and N_q are the Fermi-Dirac distribution and Bose-Einstein distribution.

The energy exchange rate can be related to the imaginary part of the phonon self-energy $\Pi''_{\mathbf{q}v}$ arising from the EPI [55].

$$E_{e-ph}(q, v) = 8\omega_q \left[N(\hbar\omega_q, T_{ph}) - N(\hbar\omega_q, T_e) \right] \text{Im} \left[\Pi''_{\mathbf{q}v} \right] \quad (7)$$

$$\Pi''_{\mathbf{q}v} = \sum_{mn, \mathbf{k}} |g_{mn}^v(\mathbf{k}, \mathbf{q})|^2 \frac{f(\varepsilon_{n\mathbf{k}}) - f(\varepsilon_{m\mathbf{k}+\mathbf{q}})}{\varepsilon_{n\mathbf{k}} - \varepsilon_{m\mathbf{k}+\mathbf{q}} - \hbar\omega_{\mathbf{q}v} + i\eta} \quad (8)$$

The EPI matrix is determined using density functional perturbation theory which is implemented in Quantum-Espresso package. The phonon self-energy due to electron-phonon coupling is calculated using electron-phonon Wannier package [55,56] which employs maximally localized Wannier functions to interpolate the EPI matrix into a dense grid.

2.2. Heat transfer model of substrate and metal contact

The thermal transport in amorphous SiO₂ substrate is considered using a Fourier heat conduction equation.

$$\frac{\partial}{\partial x} \left(k \frac{\partial T}{\partial x} \right) + \frac{\partial}{\partial y} \left(k \frac{\partial T}{\partial y} \right) - S = 0 \quad (9)$$

The electron and phonon thermal transport in metal is assumed to be diffusive, and a two-temperature model based on the diffusive heat conduction equations is employed.

$$\frac{\partial}{\partial x} \left(k_e \frac{\partial T_e}{\partial x} \right) + \frac{\partial}{\partial y} \left(k_e \frac{\partial T_e}{\partial y} \right) - \dot{Q}_{e-ph} + S = 0 \quad (10)$$

$$\frac{\partial}{\partial x} \left(k_{ph} \frac{\partial T_{ph}}{\partial x} \right) + \frac{\partial}{\partial y} \left(k_{ph} \frac{\partial T_{ph}}{\partial y} \right) + \dot{Q}_{e-ph} + S = 0 \quad (11)$$

Here, the source term S includes the interfacial heat flux. The energy exchange rate between the electrons and phonons depend on the coupling constant and the electron and phonon temperature difference [47].

$$\dot{Q}_{e-ph} = G_{e-ph} (T_e - T_{ph}) \quad (12)$$

For materials with low Debye temperature, e.g., metals, $\hbar\omega_{\mathbf{q}v} < k_B T_e$ and $\hbar\omega_{\mathbf{q}v} \ll k_B T_{ph}$. Equation (6) can be rewritten as:

$$S(k, q) = (f_k - f_{k+q}) \frac{k_B (T_{ph} - T_e)}{\hbar\omega_{\mathbf{q}v}} \quad (13)$$

Substituting Eq. (13) into Eq. (5), one can obtain

$$E_{e-ph} = \left[4k_B \frac{2\pi}{\hbar} \sum_{mn, \mathbf{k}, v, q} |g_{mn}^v(\mathbf{k}, \mathbf{q})|^2 (f_k - f_{k+q}) \delta(\varepsilon_{m\mathbf{k}+\mathbf{q}} - \varepsilon_{n\mathbf{k}} - \hbar\omega_{\mathbf{q}v}) \right] (T_{ph} - T_e) \quad (14)$$

In this case, a constant can be defined to describe the EPI which is independent on phonon distribution

$$G_{e-ph} = 4k_B \frac{2\pi}{\hbar} \sum_{mn, \mathbf{k}, v, q} |g_{mn}^v(\mathbf{k}, \mathbf{q})|^2 (f_k - f_{k+q}) \delta(\varepsilon_{m\mathbf{k}+\mathbf{q}} - \varepsilon_{n\mathbf{k}} - \hbar\omega_{\mathbf{q}v}) \quad (15)$$

Finally, the electron-phonon energy exchange rate in Eq. (14) can be written in the form of Eq. (12) for metal contact.

2.3. Interface coupling and boundary conditions

The interfaces considered in this model include the graphene/Cu and graphene/substrate interfaces. At graphene/Cu interfaces, both electrons and phonons can carry heat, and their heat flux is determined by Refs. [57,58].

$$J_e = \int_0^\infty \frac{1}{2\pi\hbar} (E - \mu) (f_F(E, T_1) - f_F(E, T_2)) \zeta_e(E) dE \quad (16)$$

$$J_{ph} = \int_0^\infty \frac{\hbar\omega}{2\pi} (f_B(\omega, T_1) - f_B(\omega, T_2)) \zeta_{ph}(\omega) d\omega \quad (17)$$

where ζ_e and ζ_{ph} are the transmission functions of electrons and phonons, respectively. The transmission functions are determined using Green's function method with DFT calculations [58,59].

At interfaces between graphene and SiO₂ substrate, only phonons contribute to the interfacial heat flux. The SiO₂ is in amorphous state, and the diffuse mismatch model [60] can be used to describe the phonon coupling at the interface between graphene and SiO₂ substrate.

$$G = \frac{1}{4} \sum_j^3 \int_0^{\omega_{Dj}} \hbar\omega v_{1j} D_1 \frac{\partial N}{\partial T} \alpha_{1-2j}(\omega) d\omega \quad (18)$$

where α_{1-2j} is the transmission probability of phonon polarization j from material 1 (graphene) to material 2 (SiO₂). D_1 is the phonon DOS of material 1, and N is the Bose-Einstein distribution of phonons. The transmission probability can be evaluated using diffuse mismatch model

$$\alpha_{1-2j}(\omega) = \frac{v_{2j} D_{2j}(\omega)}{v_{1j} D_{1j}(\omega) + v_{2j} D_{2j}(\omega)} \quad (19)$$

The effective DOS of graphene is evaluated using $D_{eff}(\omega) = \omega/2\pi t v_{1j}^2$ where the c -axis velocities of graphite are used for v_{1j} [60]. The DOS of SiO₂ is evaluated using a sine dispersion curves $\omega_j = \omega_{Dj} \sin(\pi k/2k_{Dj})$ with a cutoff wave vector determined by Debye temperature $k_{Dj} = k_B \Theta_D / \hbar v_{2j}$ [18]. The TBC at SLG/SiO₂ and SLG/Cu interfaces are predicted and compared with the available experimental data in literature, and detailed discussion can be found in the supplementary document.

In Fig. 1, boundary conditions for SLG, Cu contacts, and SiO₂

substrate have been specified. Since the thickness of SLG is very small (0.335 nm), the heat flux at SLG edges is neglected, and the reflecting boundary condition with assumption of specular reflection is applied for the phonons escaping the domain. For solving Fourier heat conduction equations for Cu contact and SiO₂ substrate, constant temperature (300 K) boundary conditions are applied. The source term in phonon BTE equation is specified by the electron-phonon energy exchange, and the heat exchange by both electrons and phonons are considered at the interfaces. The electron diffusion equation (1) and phonon BTE equation (2) are discretized using the finite volume method, and the nonlinear equations are solved using Newton-Raphson method. The flow chart of the numerical implementation of the governing equations is shown in Fig. 2. The convergence criterion is set at 10^{-5} for the temperature residual. The difference between the heating power and the total heat transfer rate is also examined for the convergence. The total heat transfer rate includes the heat transferred through the SLG/SiO₂ interface by phonons and through the SLG/Cu interface by both electrons and phonons.

3. Results and discussion

3.1. Electron phonon interaction strength in graphene

The phonon self-energy $\Pi''_{\mathbf{q}\nu}$ for EPI can be determined using Eq. (8) using DFT calculations. The imaginary part of $\Pi''_{\mathbf{q}\nu}$ is a measure of the electron-phonon scattering rate. The polarization and wave-vector dependent imaginary parts of $\Pi''_{\mathbf{q}\nu}$ are calculated at different electron temperatures (100 K–3000 K) which are used in Eq. (7) for the calculation of energy exchange rates between electrons and phonons. The DFT calculations to estimate $\Pi''_{\mathbf{q}\nu}$ are performed at electron temperature ranging from 100 K to 3000 K with an interval of 100 K. Linear interpolation is employed to determine $\Pi''_{\mathbf{q}\nu}$ at an arbitrary electron temperature during the iterative solution of electron/phonon temperature using hybrid BTE model. The imaginary parts of $\Pi''_{\mathbf{q}\nu}$ are plotted and discussed for different phonon modes in the first Brillouin zone (FBZ) in Fig. 3. Since the

EPI strength is nearly zero for most wave vectors in the FBZ except for the region near Γ , K and K' points, the contour plots in these figures only show the region within a radius of $\delta q/q_0 < 0.1$, where $\delta q = q - q_j$ with $j = \Gamma, K, \text{ or } K'$ and $q_0 = 2\pi/a$.

As shown in Fig. 3, the self-energy is non-zero for LO, TO and LA modes, while the self-energy of TA, ZA, and ZO phonons is negligible. Fig. 3 (a) and (b) shows that the interaction between LO phonons and electrons is focused in a small region around Γ point. As shown in Fig. 3 (c) and (d), the self-energy of TO phonons is noticeable in the region around Γ point, and it also has small values in the regions near K and K'. Comparing with Fig. 3 (a) and (b), the peak values of the imaginary part of $\Pi''_{\mathbf{q}\nu}$ for TO modes are about 3 times larger than that of LO modes. Fig. 3 (e) and (f) indicates that the self-energy of LA phonons is one order of magnitude smaller than that of LO and TO phonons, and it is non-negligible only around K and K' points. As the temperature increases from 300 K to 1500 K, the magnitude of self-energy becomes larger, and the regime with non-zero values in FBZ also becomes larger for each of the LO, TO, and LA phonons.

3.2. Heat dissipation in suspended SLG without Cu contact (system I)

Fig. 4 shows the temperature profiles for electrons and phonons along the SLG with different length. In the SLG, electrons can only transfer heat to phonons. If the SLG length L is small, electrons and phonons are in high non-equilibrium: electron temperature is high while phonon temperature is low. Since the thermal resistance along the SLG is small, the electron and phonon temperatures are quite uniform in SLG at small L , e.g., for $L=24.5$ nm as shown in Fig. 4 (a) and (b). As L increases, electrons and phonons tend to equilibrate with each other: electron temperature drops while phonon temperature increases. As shown in Fig. 4 (a), electron temperature drops as L increases from 24.5 nm to 245 nm, but the temperature at the center of SLG ($x = 0$) changes little after $L > 73.5$ nm. This is because electrons receive heat only around the SLG center and lose the heat to phonons along the entire SLG. It can be an analogy to the heat transfer in a one-dimension fin, and further increase of L

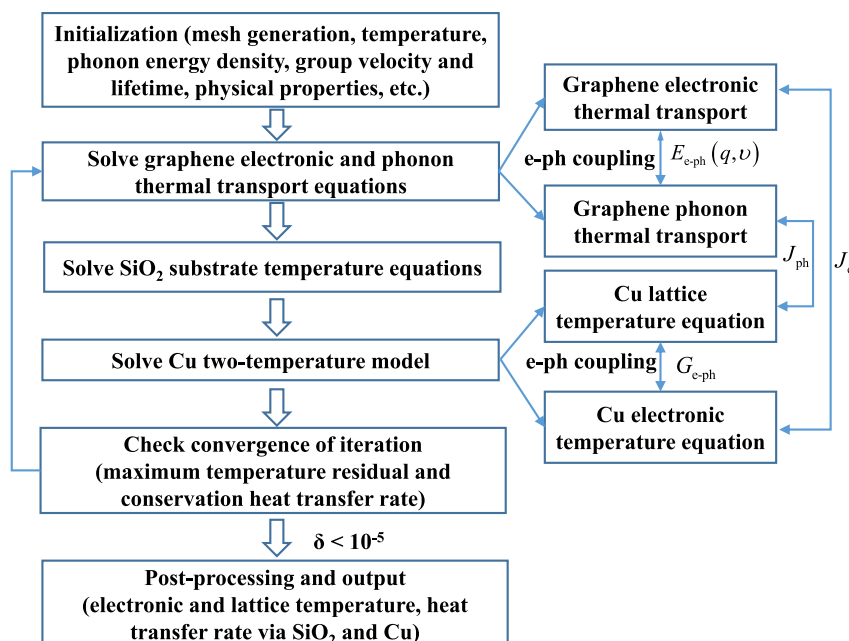


Fig. 2. Flow chart showing the implementation of the hybrid model. (A colour version of this figure can be viewed online.)

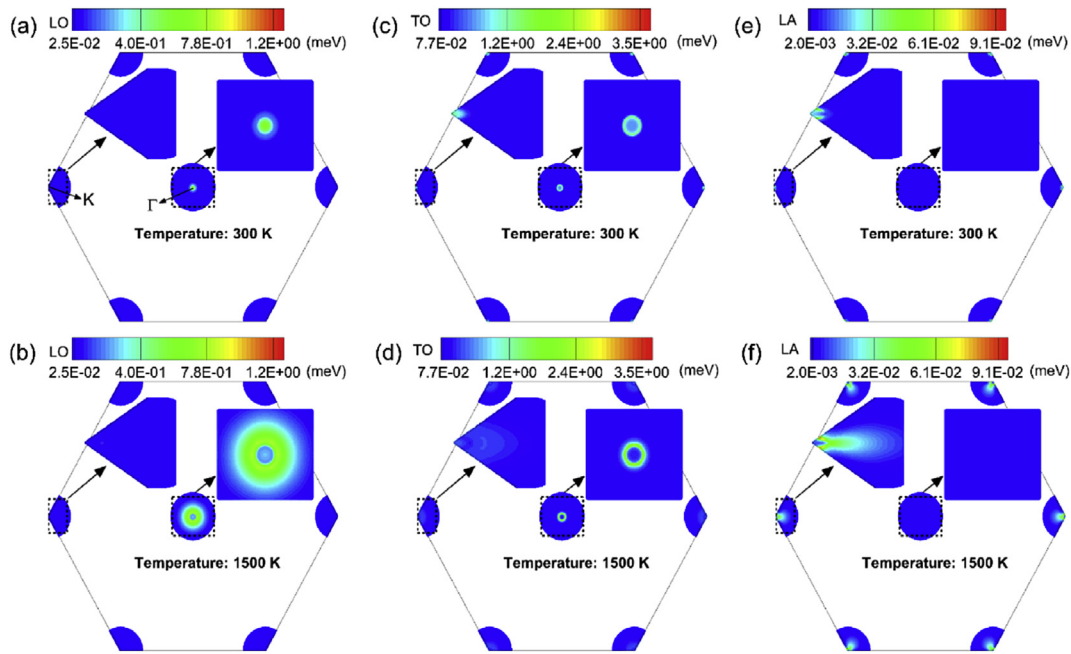


Fig. 3. Imaginary part of phonon self-energy in the first Brillouin zone with different electron temperatures: (a) LO mode at 300 K; (b) LO mode at 1500 K; (c) TO mode at 300 K; (d) TO mode at 1500 K; (e) LA mode at 300 K; (f) LA mode at 1500 K. As denoted in (a), Γ point is the zone center while K point is the corner of the first Brillouin zone. (A colour version of this figure can be viewed online.)

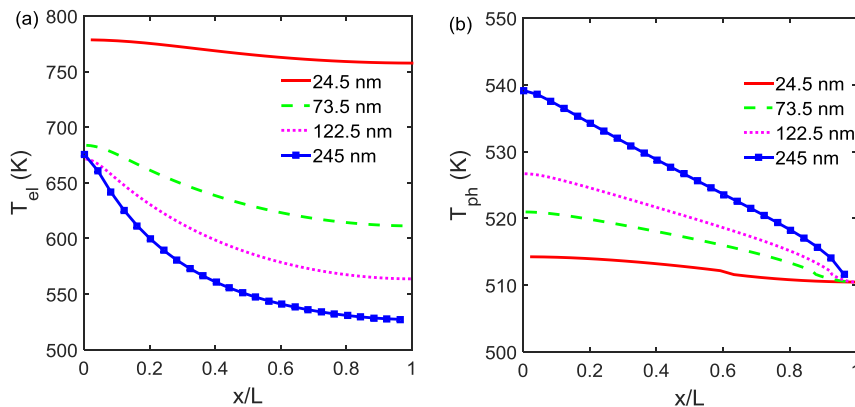


Fig. 4. (a) Electron and (b) phonon temperature profiles along SLG with different length in System I: SLG suspended on SiO_2 as shown in Fig. 1 (a). The x -axis is normalized with their SLG length, while the legend denotes different SLG length. The heating power is 0.04 mW. (A colour version of this figure can be viewed online.)

beyond certain values cannot help to reduce the temperature in the center.

On the contrary, the phonon temperature along the SLG increases as L increases from 24.5 nm to 245 nm as shown in Fig. 4 (b). It can be also observed that the phonon temperature at $x = 0$ increases faster as L increases. This is because phonons receive heat from electrons along the entire SLG but can only transfer heat near its edge contacting with SiO_2 . The thermal resistance of SLG for heat dissipation increases with the SLG length, which leads to a higher phonon temperature in SLG as shown in Fig. 4 (b).

3.3. Heat dissipation in suspended SLG with Cu contact (system II)

Fig. 5 (a) and (b) shows the temperature profiles along the SLG in System II for electrons and phonons, respectively. The suspended SLG in System II can dissipate heat to both Cu and SiO_2 near the edge, *i.e.*, $x/L = \pm 1$. At a small L , electrons and phonons in the SLG

are at a highly non-equilibrium state: the electron temperature is high while phonon temperature is low. The heat absorbed by electrons is mainly dissipated to Cu contacts directly, and only a small portion is transferred to phonons in SLG. The heat dissipation at the SLG/ SiO_2 interface is inefficient due to the low phonon temperature. Therefore, the SLG/Cu interface is the major heat dissipation pathway for the SLG with a small L as shown in Fig. 6 (a) and (b).

As L increases, electrons and phonons equilibrate, and more heat is transferred to phonons in the SLG. At a larger L , electron temperature becomes smaller and phonon temperature increases near the contact region with SiO_2 and Cu, as shown in Fig. 5 (b). Therefore, the heat dissipation at SLG/Cu interfaces decreases while the heat dissipation at SLG/ SiO_2 interfaces increases, as shown in Fig. 6 (a) and (b).

It can be observed from Fig. 6 (b) that the heat dissipation at SLG/Cu interfaces is larger than that at SLG/ SiO_2 interfaces as

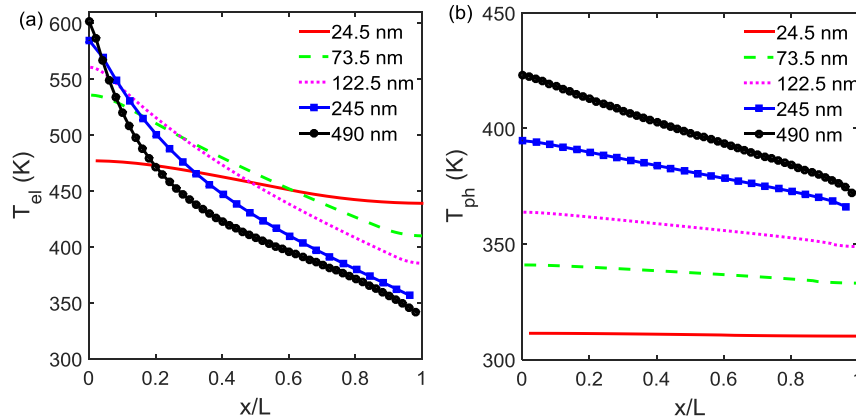


Fig. 5. (a) Electron and (b) phonon temperature profiles along SLG with different length in System II: SLG suspended on SiO₂ with Cu contacts as shown in Fig. 1 (b). The x-axis is normalized with their SLG length, while the legend denotes different SLG length. The heating power is 0.04 mW. (A colour version of this figure can be viewed online.)

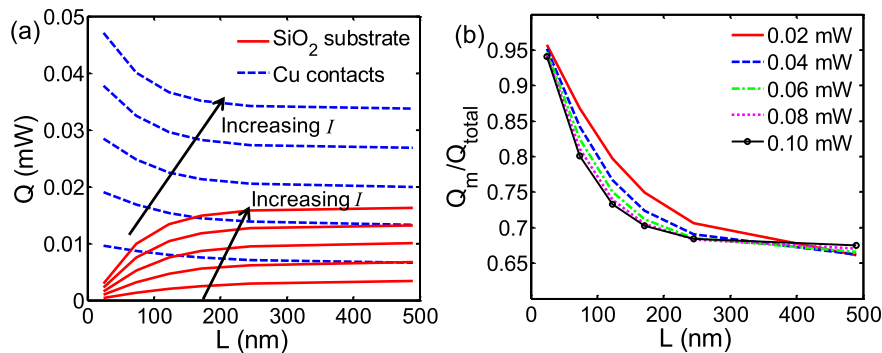


Fig. 6. Heat dissipation pathways in Structure II: SLG suspended on SiO₂ with Cu contacts as shown in Fig. 1 (b). (a) Heat transfer rate via SiO₂ and Cu as a function of SLG length. The arrows show the direction of increasing heating power from 0.02 mW to 0.1 mW with an interval of 0.02 mW. (b) Ratio of heat transfer rate via Cu contacts to total heating power as a function of SLG length. The legend denotes different heating power. (A colour version of this figure can be viewed online.)

indicated by the $Q_m/Q_{total} \approx 0.65$ for large L . Since the contact length of SLG with Cu and SiO₂ are same in System II, the heat dissipation at SLG/Cu and SLG/SiO₂ interfaces are determined by their TBC and temperature difference. It is worth noting that the TBC at SLG/SiO₂ interface is larger than that at SLG/Cu interface as demonstrated by recent measurements [15,61] and numerical predictions [50,62,63]. The predictions of TBC in present study are shown in Fig. S1 of the supplementary material. The temperature difference at SLG/Cu interfaces should be large than that at SLG/SiO₂ interfaces. This is confirmed by comparing the maximum

temperature in Cu and SiO₂ contacts in Fig. 7 (a) and (b) with the SLG temperature near contact in Fig. 5 (b). In Fig. 7, L denotes the SLG length while the arrows show the direction of increasing heating power from 0.02 mW to 0.1 mW with an interval of 0.02 mW. The maximum temperature in SiO₂ is well above the boundary temperature of 300 K at a large SLG length L while the maximum temperature in Cu is close to 300 K for all the heating power and SLG length L considered. This is because the low thermal conductivity of SiO₂ deteriorates the heat conduction and leads to a large thermal resistance as well as a large temperature gradient in SiO₂. Therefore, SLG/Cu interface can still be an effective heat dissipation pathway if its contact area is comparable to that of SLG/SiO₂ interfaces, even though it has lower TBC than SLG/SiO₂ interface.

3.4. Heat dissipation in supported SLG without Cu contact (system III)

In System III, the SLG is fully supported on SiO₂ substrate as shown in Fig. 1 (c). The heat absorbed by electrons can only be transferred to phonons in SLG, followed by the heat dissipation to the SiO₂ substrate via phonons. As shown in Fig. 8 (a) and (b), both electron and phonon temperatures decrease as the SLG length increases for System III. This is comprehensible because the heating power is fixed while the heat transfer area between SLG and SiO₂ substrate increases as the SLG length increases. This trend is larger for the SLG with a small length, e.g., from 24.5 nm to 73.5 nm.

Moreover, the temperature distribution is nearly uniform in SLG

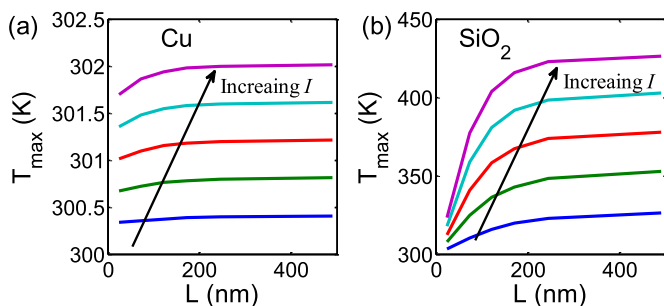


Fig. 7. Variations of maximum temperature in (a) Cu contact and (b) SiO₂ contact as a function of SLG length in Structure II: SLG suspended on SiO₂ with Cu contacts as shown in Fig. 1 (b). The arrows show the direction of increasing heating power from 0.02 mW to 0.1 mW with an interval of 0.02 mW. (A colour version of this figure can be viewed online.)

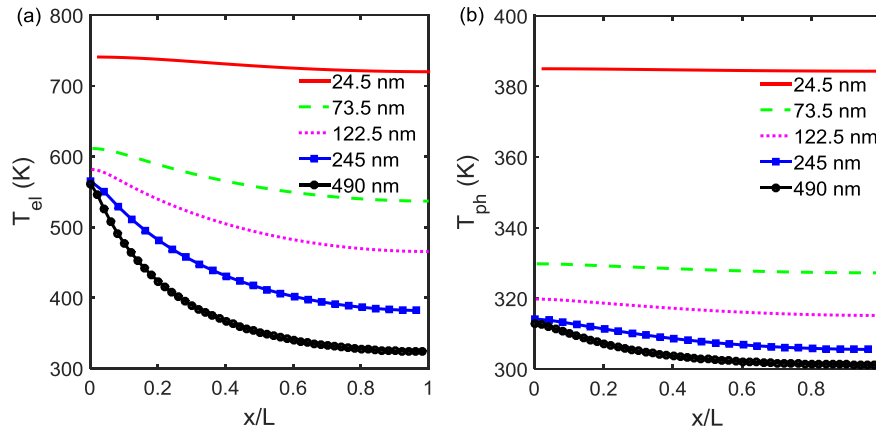


Fig. 8. (a) Electron and (b) phonon temperature profiles along SLG with different length in System III: SLG supported on SiO₂ substrate as shown in Fig. 1 (c). The x-axis is normalized with their SLG length; the legend denotes different SLG length. The heating power is 0.04 mW. (A colour version of this figure can be viewed online.)

with a small length, e.g., $L=24.5$ nm in Fig. 8 (a) and (b). This is because heat can spread efficiently in the small SLG due to the high thermal conductivity. Meanwhile, electrons and phonons are in high non-equilibrium in the SLG of a small length. Therefore, the heat dissipation in the small length SLG behaves like the heat transfer between heat reservoirs with thermal resistances in series: the thermal resistance R_{e-ph} for the electron-phonon heat exchange, and the contact resistance R_{subs} between SLG and SiO₂ substrate. As the SLG length increases, the temperature drop along SLG increases for both electrons and phonons. The electrons and phonons can approximately reach thermal equilibrium state in the region far away from the heating zone at the center for a large length SLG, e.g., $L=490$ nm.

3.5. Heat dissipation in supported SLG with Cu contact (system IV)

Compared with the SLG in System III, the SLG in System IV has contacts with Cu in addition to the contact with SiO₂ substrate, as shown in Fig. 1 (d). The electrons in SLG can transfer heat to phonons in SLG as well as the electrons in Cu contacts through the SLG/Cu interfaces. This pathway via Cu contacts can have significant impact on the heat dissipation in the SLG of short length.

Comparing the electron temperature in Fig. 8 (a) and Fig. 9 (a), it can be observed that the electron temperature is lower in SLG with L of 24.5 nm and 73.5 nm. Similar trend can be observed for phonon temperature in Fig. 8 (b) and Fig. 9 (b) for SLG with L of 24.5 nm and 73.5 nm. However, the magnitude and distribution of both electron

and phonon temperature remain similar as the SLG in System III of large L , e.g., 245 nm and 490 nm, no matter whether the SLG has Cu contacts or not. This is because SLG/SiO₂ interfaces become the major heat transfer pathway for the SLG with a large length. In this situation, most of the heat is dissipated into SiO₂ substrate via the electron-phonon-SiO₂ path, and then electrons reach thermal equilibrium with phonons near the edges of SLG.

Fig. 10 (a) shows the variations of heat transfer rate via SiO₂ substrate and Cu contacts as a function of SLG length in System IV for different heating power. As shown in Fig. 10 (a), the heat dissipation at SLG/Cu interfaces dominates at a small SLG length, but decreases as the SLG length increases, and finally becomes negligible for the large SLG length above 490 nm. The heat dissipation at SLG/SiO₂ interfaces has an opposite trend when SLG length increases. Fig. 10 (b) shows the ratio of heat transfer rate Q_m at the SLG/Cu interface to the total heat transfer rate Q_{total} . It clearly shows that the major heat dissipation pathway is switched from the SLG/Cu interface to the SLG/SiO₂ interface as the SLG length increases for all heating power considered. It can be also observed, in Fig. 10 (b), that Q_m/Q_{total} decreases with increasing heating power for a constant SLG length. This is because the electron-phonon heat exchange is enhanced at higher temperature due to the increased EPI strength as shown in Fig. 3.

3.6. Discussion of the heat transfer pathways in SLG nanostructures

The maximum temperature in SLG is an important parameter to

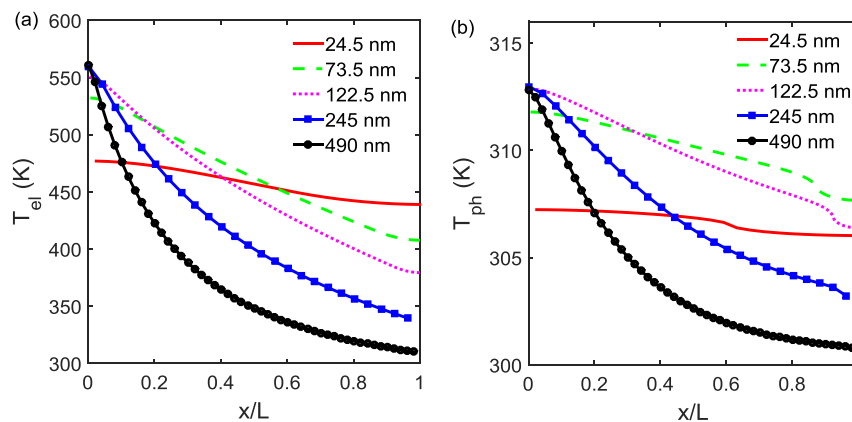


Fig. 9. (a) Electron and (b) phonon temperature profiles along SLG with different length in System IV: SLG supported on SiO₂ substrate with Cu contacts as shown in Fig. 1 (d). The x-axis is normalized with their SLG length; the legend denotes different SLG length. The heating power is 0.04 mW. (A colour version of this figure can be viewed online.)

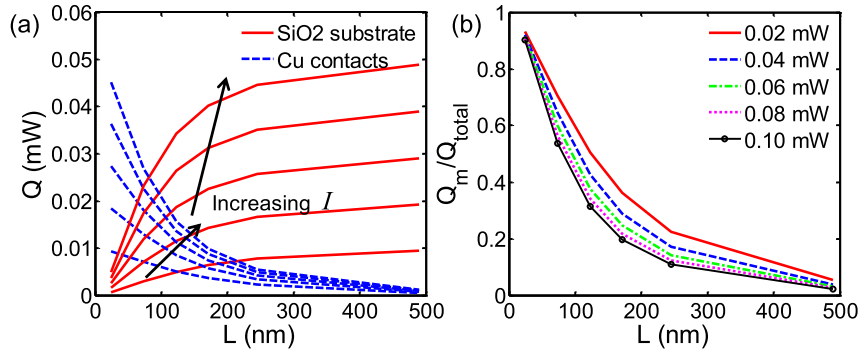


Fig. 10. Heat dissipation pathways in Structure IV: SLG supported on SiO₂ with Cu contacts as shown in Fig. 1 (d). (a) Heat transfer rate via SiO₂ and Cu as a function of SLG length. The arrows show the direction of increasing heating power from 0.02 mW to 0.1 mW with an interval of 0.02 mW. (b) Ratio of heat transfer rate via Cu contacts to the total heating power as a function of SLG length. The legend denotes different heating power. (A colour version of this figure can be viewed online.)

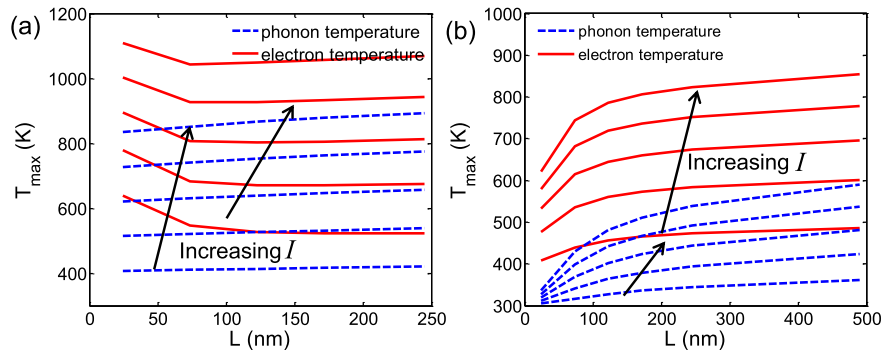


Fig. 11. Electron and phonon temperatures at the center of SLG with different lengths for (a) System I and (b) System II. The arrows show the direction of increasing heating power from 0.02 mW to 0.1 mW with an interval of 0.02 mW. (A colour version of this figure can be viewed online.)

consider for both efficient thermal management and improving reliability of the SLG electronic devices. The maximum temperature occurs at the center of SLG for all systems as expected. The peak temperature, T_{max} , is shown in Fig. 11 (a) and (b) as a function of SLG length at different heating power for System I and II, respectively. Due to the electron-phonon non-equilibrium, electron temperature is high while phonon temperature is low at $x = 0$ in the SLG of a small L in System I, as shown in Fig. 11 (a). It can be also seen that the maximum electron temperature (at $x = 0$) increases slowly as L increases beyond a certain value, e.g., 73.5 nm for $I > 0.08$ mW. In System II, the SLG/Cu interface is an important heat dissipation pathway for both electrons and phonons at a small L . So as L increases, the maximum electron and phonon temperatures increase

faster when L is small, and then increase with a smaller rate, as shown in Fig. 11 (b).

In System III and IV, the peak temperature is shown in Fig. 12 (a) and (b) as a function of SLG length at different heating power. In System III, the peak temperatures of electrons and phonons drop quickly as the SLG length increases, and then remain nearly constant after $L > 100$ nm. This is simply because the SLG/SiO₂ interface is the only heat dissipation pathway and the interface area increases with the SLG length.

However, the SLG/Cu interface is the major heat dissipation pathway when SLG length is small in System IV. The thermal energy is mainly stored in electrons due to the high non-equilibrium between electrons and phonons. As the SLG length increases, the

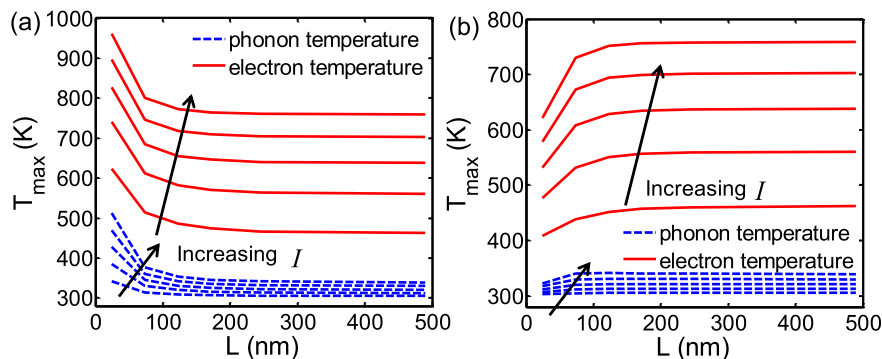


Fig. 12. Electron and phonon temperatures at the center of SLG with different length for (a) System III and (b) System IV. The arrows show the direction of increasing heating power from 0.02 mW to 0.1 mW with an interval of 0.02 mW. (A colour version of this figure can be viewed online.)

heat dissipation at SLG/Cu interfaces decreases rapidly as shown in Fig. 10, and the temperatures of electrons and phonons at SLG/Cu interfaces also decrease. The increase of resistance from center to SLG/Cu contact cannot be compensated by the decrease in resistance due to increased SLG/SiO₂ contact length. As a result, the peak temperatures in System IV increase with SLG length when $L < 100$ nm. At a large SLG length, the heat dissipation at the SLG/Cu interface becomes negligible (see Fig. 10), and therefore the peak temperature saturates as shown in Fig. 12 (b).

4. Conclusions

In summary, the electron-phonon coupled thermal transport is modeled in the suspended or supported SLG with/without Cu contacts. Using first-principle calculations, the EPI strength of different phonon modes are obtained at different temperatures. The k -space distribution of EPI strength shows that the EPI is strong for LO and TO modes, moderate for LA modes, and negligible for TA, ZA, and ZO modes. The EPI strength increases with temperature, which indicates the enhanced electron-phonon heat exchange at high temperature.

The maximum temperature in SLG and the role of SLG/Cu and SLG/SiO₂ interfaces in the heat dissipation depend on both the SLG support configuration and the SLG length. The SLG/Cu interface is an important heat dissipation pathway for both electrons and phonons in the suspended SLG with Cu contact, and it can significantly improve the heat dissipation and lower the SLG temperature compared with that of SLG suspended on SiO₂ without Cu contact. The SLG/Cu interface can be the major heat dissipation pathway when its contact area is comparable to that of SLG/SiO₂ interface, which can be attributed to the higher thermal conductivity of Cu. The presence of Cu contact can be effective in lowering the temperature in supported SLG on SiO₂ only when SLG length is small. When the SLG length is large in the supported SLG on SiO₂ with Cu contact at ends, the SLG/SiO₂ interface becomes the major heat dissipation pathway while the heat transfer at the SLG/Cu interface becomes negligible. Due to the increased EPI strength in graphene at a higher temperature, the electron-phonon heat exchange is enhanced, and the percentage of heat dissipated through the Cu contact decreases at a high heating power. The findings in this work can provide critical insights into the electron-phonon coupled thermal transport in graphene nanostructures, and benefit the efficient thermal management of graphene nano-electronics.

Appendix A. Supplementary data

Supplementary data related to this article can be found at <http://dx.doi.org/10.1016/j.carbon.2017.07.095>.

References

- [1] A.A. Balandin, S. Ghosh, W.Z. Bao, I. Calizo, D. Teweldebrhan, F. Miao, et al., Superior thermal conductivity of single-layer graphene, *Nano Lett.* 8 (3) (2008) 902–907.
- [2] W.W. Cai, A.L. Moore, Y.W. Zhu, X.S. Li, S.S. Chen, L. Shi, et al., Thermal transport in suspended and supported monolayer graphene grown by chemical vapor deposition, *Nano Lett.* 10 (5) (2010) 1645–1651.
- [3] A.A. Balandin, Thermal properties of graphene, carbon nanotubes and nanostructured carbon materials, *Nat. Mater.* 10 (8) (2011) 569–581.
- [4] W.J. Evans, L. Hu, P. Koblinski, Thermal conductivity of graphene ribbons from equilibrium molecular dynamics: effect of ribbon width, edge roughness, and hydrogen termination, *Appl. Phys. Lett.* 96 (20) (2010) 203112.
- [5] L. Lindsay, D.A. Broido, N. Mingo, Flexural phonons and thermal transport in graphene, *Phys. Rev. B* 82 (11) (2010) 115427.
- [6] L.N. Denis, A.B. Alexander, Phonons and thermal transport in graphene and graphene-based materials, *Rep. Prog. Phys.* 80 (3) (2017), 036502.
- [7] D.L. Nika, A.A. Balandin, Two-dimensional phonon transport in graphene, *J. Phys. Condens. Matter An Inst. Phys. J.* 24 (23) (2012) 233203.
- [8] M.H. Bae, Z.Y. Ong, D. Estrada, Pop e. Imaging, simulation, and electrostatic control of power dissipation in graphene devices, *Nano Lett.* 10 (12) (2010) 4787–4793.
- [9] E. Pop, Energy dissipation and transport in nanoscale devices, *Nano Res.* 3 (3) (2010) 147–169.
- [10] J. Yu, G. Liu, A.V. Sumant, V. Goyal, A.A. Balandin, Graphene-on-diamond devices with increased current-carrying capacity: carbon sp²-on-sp³ technology, *Nano Lett.* 12 (3) (2012) 1603–1608.
- [11] J.H. Seol, I. Jo, A.L. Moore, L. Lindsay, Z.H. Aitken, M.T. Pettes, et al., Two-dimensional phonon transport in supported graphene, *Science* 328 (5975) (2010) 213–216.
- [12] T. Feng, X. Ruan, Z. Ye, B. Cao, Spectral phonon mean free path and thermal conductivity accumulation in defected graphene: the effects of defect type and concentration, *Phys. Rev. B* 91 (22) (2015) 224301.
- [13] S. Hu, J. Chen, N. Yang, B. Li, Thermal transport in graphene with defect and doping: phonon modes analysis, *Carbon* 116 (2017) 139–144.
- [14] Z.Y. Ong, E. Pop, Effect of substrate modes on thermal transport in supported graphene, *Phys. Rev. B* 84 (7) (2011).
- [15] J.J. Gengler, S.V. Shenogin, J.E. Bultman, A.K. Roy, A.A. Voevodin, C. Muratore, Limited thermal conductance of metal-carbon interfaces, *J. Appl. Phys.* 112 (9) (2012), 094904.
- [16] P.E. Hopkins, M. Baraket, E.V. Barnat, T.E. Beechem, S.P. Kearney, J.C. Duda, et al., Manipulating thermal conductance at metal-graphene contacts via chemical functionalization, *Nano Lett.* 12 (2) (2012) 590–595.
- [17] P.M. Norris, J.L. Smoyer, J.C. Duda, P.E. Hopkins, Prediction and measurement of thermal transport across interfaces between isotropic solids and graphitic materials, *J. Heat. Trans-T Asme* 134 (2) (2012), 020910.
- [18] A.J. Schmidt, K.C. Collins, A.J. Minnich, G. Chen, Thermal conductance and phonon transmissivity of metal-graphite interfaces, *J. Appl. Phys.* 107 (10) (2010) 104907.
- [19] D.L. Nika, A.S. Askerov, A.A. Balandin, Anomalous size dependence of the thermal conductivity of graphene ribbons, *Nano Lett.* 12 (6) (2012) 3238.
- [20] D.L. Nika, E.P. Pokatilov, A.S. Askerov, A.A. Balandin, Phonon thermal conduction in graphene: role of Umklapp and edge roughness scattering, *Phys. Rev. B* 79 (15) (2009) 155413.
- [21] D.L. Nika, E.P. Pokatilov, A.A. Balandin, Theoretical description of thermal transport in graphene: the issues of phonon cut-off frequencies and polarization branches, *Phys. Status Solidi* 248 (11) (2011) 2609–2614.
- [22] S. Ghosh, I. Calizo, D. Teweldebrhan, E.P. Pokatilov, D.L. Nika, A.A. Balandin, et al., Extremely high thermal conductivity of graphene: prospects for thermal management applications in nanoelectronic circuits, *Appl. Phys. Lett.* 92 (15) (2008) 151911.
- [23] Z.H. Ni, H.M. Wang, J. Kasim, H.M. Fan, T. Yu, Y.H. Wu, et al., Graphene thickness determination using reflection and contrast spectroscopy, *Nano Lett.* 7 (9) (2007) 2758–2763.
- [24] Z.H. Ni, Y.Y. Wang, T. Yu, Y.M. You, Z.X. Shen, Reduction of Fermi velocity in folded graphene observed by resonance Raman spectroscopy, *Phys. Rev. B* 77 (23) (2008).
- [25] P. Poncharal, A. Ayari, T. Michel, J.L. Sauvajol, Raman spectra of misoriented bilayer graphene, *Phys. Rev. B* 78 (11) (2008).
- [26] Y.M. You, Z.H. Ni, T. Yu, Z.X. Shen, Edge chirality determination of graphene by Raman spectroscopy, *Appl. Phys. Lett.* 93 (16) (2008).
- [27] T.M.G. Mohiuddin, A. Lombardo, R.R. Nair, A. Bonetti, G. Savini, R. Jalil, et al., Uniaxial strain in graphene by Raman spectroscopy: G peak splitting, Grüneisen parameters, and sample orientation, *Phys. Rev. B* 79 (20) (2009).
- [28] A. Das, S. Pisana, B. Chakraborty, S. Piscanec, S.K. Saha, U.V. Waghmare, et al., Monitoring dopants by Raman scattering in an electrochemically top-gated graphene transistor, *Nat. Nanotechnol.* 3 (4) (2008) 210–215.
- [29] S. Winnerl, M. Orlita, P. Plochocka, P. Kossacki, M. Potemski, T. Winzer, et al., Carrier relaxation in epitaxial graphene photoexcited near the Dirac point, *Phys. Rev. Lett.* 107 (23) (2011) 237401.
- [30] T. Winzer, A. Knorr, E. Malic, Carrier multiplication in graphene, *Nano Lett.* 10 (12) (2010) 4839.
- [31] D. Singh, J.Y. Murthy, T.S. Fisher, Mechanism of thermal conductivity reduction in few-layer graphene, *J. Appl. Phys.* 110 (4) (2011), 044317.
- [32] D.L. Nika, S. Ghosh, E.P. Pokatilov, A.A. Balandin, Lattice thermal conductivity of graphene flakes: comparison with bulk graphite, *Appl. Phys. Lett.* 94 (20) (2009) 203103.
- [33] J.M. Loy, J.Y. Murthy, D. Singh, A fast hybrid fourier–boltzmann transport equation solver for nongray phonon transport, *J. Heat Transf.* 135 (1) (2013), 011008.
- [34] A.K. Vallabhaneni, L. Chen, M.P. Gupta, S. Kumar, Solving non-gray Boltzmann transport equation in gallium nitride, *J. Heat Transf.* (2017), <http://dx.doi.org/10.1115/1.4036616>.
- [35] S.I. Anisimov, B.L. Kapeliovich, T.L. Perelman, Electron emission from metal surfaces exposed to ultrashort laser pulses, *Soviet J. Exp. Theor. Phys.* 66 (776) (1974) 776–781.
- [36] L. Jiang, H.L. Tsai, Improved two-temperature model and its application in ultrashort laser heating of metal films, *J. Heat Transf.* 127 (10) (2005) 1167.
- [37] A.J. Mcgaughey, M. Kaviany, Quantitative validation of the Boltzmann transport equation phonon thermal conductivity model under the single-mode relaxation time approximation, *Phys. Rev. B Condens. Matter* 20 (9) (2004), 189901(E).
- [38] A.K. Vallabhaneni, J. Loy, D. Singh, X. Ruan, J. Murthy, A study of spatially-resolved non-equilibrium in laser-irradiated graphene using Boltzmann transport equation, ASME, in: International Mechanical Engineering Congress

- and Exposition, ASME, San Diego, California, USA, 2013, p. 66095.
- [39] Sverdrup, P.G., Banerjee, K., Dai, C., Shih, W.K. Sub-continuum thermal simulations of deep sub-micron devices under ESD conditions. In: International Conference on Simulation of Semiconductor Processes and Devices; p. 54–57.
- [40] E. Pop, K.E. Goodson, Thermal phenomena in nanoscale transistors. Thermal and thermomechanical phenomena in electronic systems, in: ITherm '04 the Ninth Intersociety Conference on vol. 1, 2004, pp. 1–7.
- [41] S.V.J. Narumanchi, J.Y. Murthy, C.H. Amon, Boltzmann transport equation-based thermal modeling approaches for hotspots in microelectronics, *Heat Mass Transf.* 42 (6) (2006) 478–491.
- [42] D. Choi, N. Poudel, S.B. Cronin, L. Shi, Effects of basal-plane thermal conductivity and interface thermal conductance on the hot spot temperature in graphene electronic devices, *Appl. Phys. Lett.* (2017) 110.
- [43] K.I. Bolotin, K.J. Sikes, J. Hone, H.L. Stormer, P. Kim, Temperature-dependent transport in suspended graphene, *Phys. Rev. Lett.* 101 (9) (2008), 096802.
- [44] F. Giannazzo, S. Sonde, R.L. Nigro, E. Rimini, V. Raineri, Mapping the density of scattering centers limiting the electron mean free path in graphene, *Nano Lett.* 11 (11) (2011) 4612–4618.
- [45] S. Yigen, V. Tayari, J.O. Island, J.M. Porter, A.R. Champagne, Electronic thermal conductivity measurements in intrinsic graphene, *Phys. Rev. B Condens. Matter* 87 (24) (2013) 291–295.
- [46] A.S. Nissimagoudar, N.S. Sankeshwar, Electronic thermal conductivity and thermopower of armchair graphene nanoribbons, *Carbon* 52 (2) (2013) 201–208.
- [47] Z. Lin, L.V. Zhigilei, V. Celli, Electron-phonon coupling and electron heat capacity of metals under conditions of strong electron-phonon nonequilibrium, *Phys. Rev. B* 77 (7) (2008), 075133.
- [48] D. Singh, J.Y. Murthy, T.S. Fisher, Spectral phonon conduction and dominant scattering pathways in graphene, *J. Appl. Phys.* 110 (9) (2011) 155505.
- [49] J.M. Loy, D. Singh, J.Y. Murthy, Non-gray phonon transport using a hybrid bte-fourier solver, in: Ht2009: Proceedings of the Asme Summer Heat Transfer Conference 2009, vol. 2, 2009, pp. 601–610.
- [50] L. Chen, S. Kumar, Thermal transport in graphene supported on copper, *J. Appl. Phys.* 112 (4) (2012), 043502.
- [51] D.L. Nika, S. Ghosh, E.P. Pokatilov, A.A. Balandin, Lattice thermal conductivity of graphene flakes: comparison with bulk graphite, *Appl. Phys. Lett.* 94 (20) (2009), 203103.
- [52] Z.Y. Ong, E. Pop, Effect of substrate modes on thermal transport in supported graphene, *Phys. Rev. B* 84 (7) (2011), 075471.
- [53] P.B. Allen, Theory of thermal relaxation of electrons in metals, *Phys. Rev. Lett.* 59 (13) (1987) 1460–1463.
- [54] M. Lazzeri, S. Piscanec, F. Mauri, A.C. Ferrari, J. Robertson, Phonon linewidths and electron-phonon coupling in graphite and nanotubes, *Phys. Rev. B* 73 (15) (2006) 155426.
- [55] J. Noffsinger, F. Giustino, B.D. Malone, C.H. Park, S.G. Louie, M.L. Cohen, EPW: a program for calculating the electron-phonon coupling using maximally localized Wannier functions, *Comput. Phys. Commun.* 181 (12) (2010) 2140–2148.
- [56] F. Giustino, M.L. Cohen, S.G. Louie, Electron-phonon interaction using Wannier functions, *Phys. Rev. B* 76 (16) (2007).
- [57] M. Brandbyge, J.L. Mozos, P. Ordejón, J. Taylor, K. Stokbro, Density-functional method for nonequilibrium electron transport, *Phys. Rev. B* 65 (16) (2002) 165401.
- [58] W. Zhang, T.S. Fisher, N. Mingo, Simulation of interfacial phonon transport in Si-Ge heterostructures using an atomistic Green's function method, *J. Heat. Trans-T Asme* 129 (4) (2007) 483–491.
- [59] L. Chen, Z. Huang, S. Kumar, Impact of bonding at multi-layer graphene/metal interfaces on thermal boundary conductance, *RSC Adv.* 4 (68) (2014) 35852–35861.
- [60] J.C. Duda, J.L. Smoyer, P.M. Norris, P.E. Hopkins, Extension of the diffuse mismatch model for thermal boundary conductance between isotropic and anisotropic materials, *Appl. Phys. Lett.* 95 (3) (2009).
- [61] Z. Chen, W. Jang, W. Bao, C.N. Lau, C. Dames, Thermal contact resistance between graphene and silicon dioxide, *Appl. Phys. Lett.* 95 (16) (2009).
- [62] L. Chen, Z. Huang, S. Kumar, Phonon transmission and thermal conductance across graphene/Cu interface, *Appl. Phys. Lett.* 103 (12) (2013) 4821439.
- [63] R. Mao, B.D. Kong, C. Gong, S. Xu, T. Jayasekera, K. Cho, et al., First-principles calculation of thermal transport in metal/graphene systems, *Phys. Rev. B* 87 (16) (2013) 165410.